Experimental Studies on the Effect of Shunted Electrical Loads on the Performance of a Vibration-Based Electromagnetic Energy Harvester

Vijay B. Patil
Research Scholar
Visvesvaraya Technological University
Belagavi – 590018
India

Mahadev Sakri
Professor
Department of Mechanical Engineering
BLDEAs Vachana
Pitamaha.Dr.P.G.Halakatti
College of Engineering & Technology
Vijayapur -586101
India

At present, the researchers are grappling with the problems of maximizing the output power from a vibration-based electromagnetic energy harvester (VBEH). The parameters affecting the VBEH output power are: electrical damping ratio (ζ_e), mechanical damping ratio (ζ_m) and load impedances of shunted electrical load. Therefore, in this work, the experimental studies are carried out to study the effect of shunted electrical load on: i) the power output of VBEH and, ii) the determination of ζ_e which maximizes the output power. For this purpose, a VBEH is designed and developed to obtain high open-circuit voltage. The effect of resistive, inductive, and capacitive loads on output power of VBEH is investigated using experimental setup developed exclusively for the same. The experimental results reveal that the output power of VBEH is maximum: i) at the resonant frequency ii) when equivalent resistive load impedance equals the internal resistance of electromagnetic coil and iii) value of ζ_e is very small when compared to ζ_m.

Keywords: *Vibration-based electromagnetic energy harvester, shunted electrical load, electrical damping ratio, and mechanical damping ratio.*

1. INTRODUCTION

Vibration-based electromagnetic harvester (VBEH) converts vibration energy into electrical energy. VBEHs are based on the phenomenon of resonance and narrow band of the excitation frequency. The VBEHs are reliable, simple in manufacturing, require small or no maintenance, and are available in sizes as small as micro-level. The energy harvesters find applications in the field of health monitoring, embedded sensors in aerospace, etc. In the last few decades, the researchers have developed electromagnetic harvesters using some innovative approaches such as providing a dynamic magnifier in the conventional electromagnetic harvester, or using multi-harvesters, etc. The harvested output powers of these VBEHs are of the order of a few microwatts.

Therefore, in this work, the focus is on the maximization of the output power of a VBEH required to sustain the electrical loads. To achieve this objective, one has to use the concept of impedance matching between VBEH and electrical load to investigate the effect of parameters involved in the electromechanical coupling. While optimizing the electromagnetic harvester output power, it is necessary to have the value of mechanical damping ratio ζ_m much higher than that of the electrical damping ratio ζ_e. For this purpose, a VBEH is developed, which consists of the mechanical sub-system formed by a spring-mass-damper and an electromagnetic sub-system having a magnet and coil (in-line architecture) with the shunted electrical load. To obtain a high open-circuit voltage from the harvester, a hollow circular electrical coil is developed using a 41 gauge wire with 7790 number of turns and a NdFeB grade cylindrical magnet of 10 mm diameter and 30 mm height. The experimental setup is developed with the necessary instrumentation to carry out the following studies.

i) Determination of the values of electrical damping ratio ζ_e and mechanical damping ratio ζ_m .

ii) the effect of variation of electrical impedance on the output power of the harvester.

2. LITERATURE REVIEW

Willam and Yates [1], in their work, represented the combination of mechanical and electrical damping as equivalent to viscous damping. Willam et al. [2] and Roundy et al.[3] have developed different types of prototype devices of vibration-based electromagnetic harvesters. Stephen [4,5] has analyzed the problem of the extraction of energy from a vibrating environment for both direct mass and base excitation. Their work shows that a highly damped system would extract energy over a wide bandwidth of the frequencies. The possible behavior of an adaptive device designed to operate within the available amplitude environment was also considered. The transfer of maximum power within electrical, mechanical, and electromechanical systems was studied. Spreemann et al. [6] developed an analytical expression for the magnetic field of a cylindrical permanent magnet used in VBEH. The realistic performance of the VBEH, in terms of output voltage, output power, and availability, was studied. Ooi et al. [7], in their work, have discussed a method of changing the value of

Received: April 2020, Accepted: September 2020
Correspondence to: Vijay B. Patil
Research Scholar, Visvesvaraya Technological University, Belgavi, India
E-mail: vijaypatil2005@rediffmail.com
doi: 10.5937/fme2101163V

electrical damping in a vibration cycle to enhance the operational bandwidth of a VBEH. Szabo et al. [8], Nafair et al. [9] have discussed various methods of converting one form of energy to another. They designed a VBEH based on different coupling architectures operating in the low frequencies of excitation (0 to 100 HZ). Halim et al. [10,11] have shown that the electrical damping ratio may be adjusted by varying the resistive load to achieve the maximum power output. The damping characteristics of the electromagnetic harvester system are determined by using an impulse response. Zhang et al. [12] investigated the effect of ohmic resistors, rectifiers, and capacitors on electromagnetic harvested performance. They showed that the electromagnetic harvester performance using pure resistive load could not be generalized in all applications. Tai and Zuo [13] carried out the optimization for a maximum power of a VBEH through electrical load or electrical damping ratio and excitation frequency using two variable optimization analysis. Their work showed that the optimal electrical damping ratio is always larger than the mechanical damping ratio. Caruso [14] analyzed the electromagnetic harvester shunted to a resonant electric circuit, under harmonic excitation. Their work showed that a constant level of the harvester power can be achieved, under resonant excitation. Ashraf et al. [15] through their findings presented the method of improved energy harvesting from low-frequency vibrations and showed that the resonance amplification at multiple frequencies can improve the efficiency of harvesting energy from broadband vibrations. Simeone et al. [16] proposed a new strategy to obtain maximum power from an electromagnetic energy harvester by adjusting the electrical load according to the input level at the steady-state condition. They also showed that if the electrical load is tuned according to the level of harmonic excitation, then the harvester can always operate at the optimum conditions. Zuo and Cui [17] discussed about the dual-functional energy harvesting and vibration control. In their work, the viscous damping element between the tuned mass damper and the primary system is replaced by an electromagnetic transducer shunted to a resonant RLC Circuit. Using this concept, they showed that the vibration of the primary system can be minimized and the harvested electrical power maximized. Liu et al. [18] have derived ready to use analytical tuning laws for energy harvesting series electromagnetic tuned mass dampers. The numerical analysis showed that such a system can achieve enhanced performance in the form of both vibration control of the primary system and energy harvesting due to tuning of the resonance of the mechanical system and the electrical system. Tang and Zuo [19] in their work have showed that, theoretically, the energy harvesting can go to infinite value and state that a reasonably large electrical damping in dual-mass harvester can achieve more energy harvesting. Gilani [20] has developed a VBEH for an industrial centrifugal pump with a consideration that the VBEH will be an integral part of the autonomous vibration monitoring system. Tadesse et al. [21] have proposed and developed a multi-modal harvesting system or hybrid energy harvesting system to enhance the efficiency of mechanical energy harvesting and to improve the functionality of the electromagnetic harvesting system over the wide excitation frequency range. Bhatnagar and Owende [22] have presented the characteristics of common energy harvesting transducers and typical power density of ambient energy sources. Wang et al. [23-25] have reviewed available energy harvesting techniques that can be used for roadway and bridge for different applications and have given some suggestions for the research work in the area of energy harvesters. Zuo and Zhang [26] have presented a comprehensive assessment of the power that is available for harvesting in the vehicle suspension system. The road tests of the vehicle conducted to evaluate the energy potential and to verify the analytical results on vehicle suspension displacement, velocity, and energy. The effect of vehicle speed on harvested power is investigated. Chamanian et al. [27] have developed an electromagnetic energy harvester to be used in a wireless sensor node system for charging its rechargeable batteries while the system is operational. Yildrim et al. [28], EI-Sayed et al. [29], carried out an extensive literature review covering the development in the design of VBEH and piezoelectric harvesters with various configurations and applications, and various techniques such as the use of a mechanical amplifier, multimodal arrays, etc., for enhancing the harvested power and widening of operation range. Malaji and Ali [30], Wang et al.[31], and Siang et al. [32] have carried out research studies on the methods of enhancing harvester output power, using different electrical coil and magnet system configurations.

This literature review reveals that only a few studies have been carried out on the effect of ohmic load or matched load on the power harvested from a VBEH. Hence, in this work, experimental studies are carried out to study the effect of various types of shunted electrical loads on the performance of a VBEH. Since the average generated power P_{ave} depends predominantly on the electrical damping ratio ζ_e, and the value of ζ_e is determined by transient open circuit response and the loaded impulse response of the developed VBEH. The value of ζ_e is also calculated using the theoretical relation developed by Spreemann et al. [6]

3. VIBRATION BASED ELECTROMAGNETIC HARVESTER (VBEH)

The vibration-based electromagnetic harvester as shown in Fig. 1, is a single degree of freedom (SDOF) system consisting of mass *(m)*, spring *(k),* and damper *(c)* subjected to sinusoidal base excitation *y(t).* In this system: $c = c_m + c_e$ where c_m = mechanical damping coefficient and c_e = electrical damping coefficient.

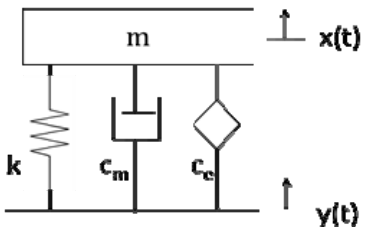

Figure 1: Schematic of Single Degree of Freedom (SDOF) VBEH

The displacement of harvester mass is *x(t).* The relative displacement $z(t)$ between the mass and the base

is $[x(t) - y(t)]$ and the base displacement $y(t)$ is equal to $Y\sin(\omega t)$, where ω is the circular excitation frequency. The governing equation of the harvester system is:

$$m\ddot{z} + c\dot{z} + kz = -m\ddot{y} \tag{1}$$

The average generated power P_{ave} from VBEH is calculated using Eq.(2) given by William et al. [1,2]

$$P_{ave} = \frac{m\zeta_e \left(\frac{\omega}{\omega_n}\right)^3 \omega^3 Y^2}{\left(1-\left(\frac{\omega}{\omega_n}\right)^2\right)^2 + \left(2\left(\zeta_e+\zeta_m\right)\frac{\omega}{\omega_n}\right)^2} \tag{2}$$

where, the electrical damping ratio $\zeta_e = \frac{c_e}{c_c}$, the mechanical damping ratio $\zeta_m = \frac{c_m}{c_c}$, the critical damping coefficient is c_c, and circular natural frequency of a mechanical sub-system is ω_n.

4. EXPERIMENTAL SETUP: VBEH SHUNTED TO ELECTRICAL LOADS)

In this section, the experimental setup developed for the measurement of average harvested power P_{aveh} from VBEH is described. Figure 2 shows a schematic VBEH shunted to an electrical load circuit composed of an inductance L, resistance R_L, and capacitance C

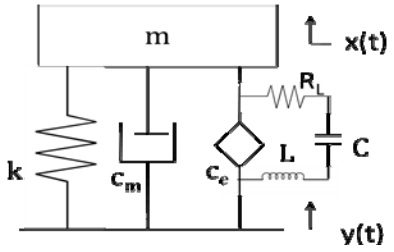

Figure 2. Schematic of VBEH with shunted electrical load

This schematic of VBEH is converted into an experimental setup. In this setup, the mechanical sub-system and electrical coil-magnet sub-system with magnet holding devices are as shown in Fig.3. Figure 4 shows the overall experimental setup of VBEH equipped with a mechanical sub-system and electrical sub-system shunted to a resonant electric circuit.

In the setup, a DC motor is mounted on the base frame. A Cam - follower system is placed on the shaft of the DC motor to convert rotary motion into simple harmonic motion. The amplitude of base excitation of 1mm is provided by adjusting the cam eccentricity, and the frequency of excitation varied by changing the speed of DC motor drive. The plate representing the mass 'm' moves, within linear bearings, between two parallel guide rods. The upper end of spring is connected to the mass plate, and the lower end of the spring is connected to the wooden support. The electrical coil is fixed on the wooden support, and the magnet is attached to the mass plate to obtain relative motion $z(t)$ between the coil and magnet. Displacement response of the harvester mass is measured by using the ultrasonic displacement sensor, and a proximity speed sensor measures the speed of the DC drive motor. These sensors are connected to a computer through an Arduino device to get the records of the response.

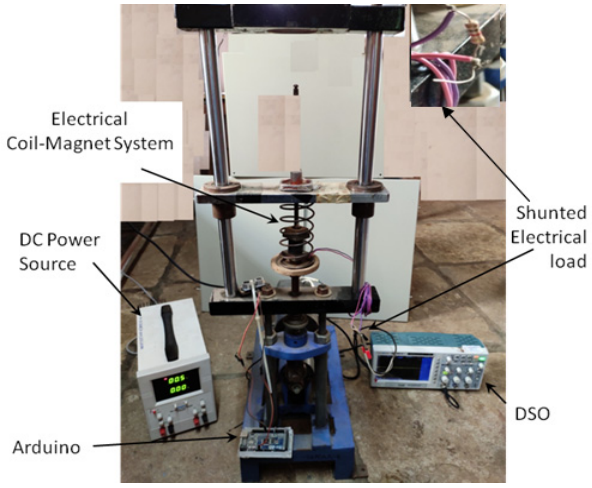

Figure 3. Overall Experimental Setup

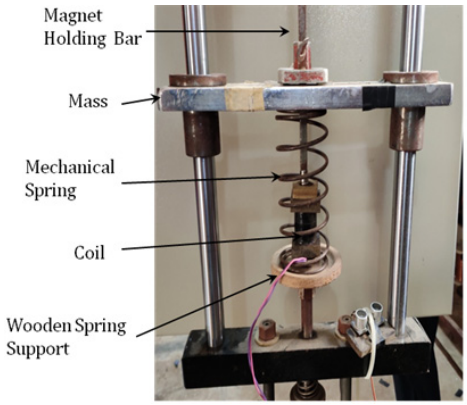

Figure 4. Spring-Mass with Magnet Holding Device

4.1 Design of electrical coil-magnet system (in-line architecture)

A cylindrical magnet moves in an electrical coil in the direction of motion, as shown in Fig. 5.

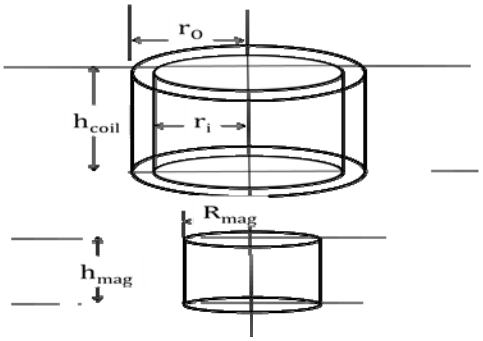

Figure 5. Magnet and coil (in-line configuration)

To get high open-circuit voltage output, an electrical coil, as shown in Fig.6, is developed using a small diameter copper wire and with a high value of the total number of turns. For this purpose, a copper coil is fabricated with wire diameter d_{co} = 0.089 mm (41 gauge), coil height h_{coil} = 30 mm, inner radius r_i = 8 mm, and outer radius r_0 = 11 mm, mean radius r_m = 9 mm. Selecting the coil inductance L_{coil} as 0.45H (Hennery) and using the Wheelers approximation formula

[33], the total number of turns N_{total} comes out to be 7790, and the copper fill factor k_{co} as 0.06522. The number of longitudinal turns N_{long} and the number of lateral turns N_{lat} are as 342 and 22.80, respectively.

Figure 6. Developed coil

The resistance of the coil R_c is determined using Eq. (3) [11]:

$$R_c = \frac{4\rho\left(r_0^2 - r_1^2\right)h_{coil}}{a^2} = 1814\Omega \qquad (3)$$

where ρ is the specific resistivity of the copper wire material = 1.72×10^{-8}, Ωm and a is the cross-sectional area of wire = 8.04×10^{-9} m^2. However, the measured value of R_c was found to be 1620Ω. The difference between the theoretical and experimental value of the internal resistance of the coil may be due to the coil winding method and calculating the number of turns of the coil. With this value of R_c, the final specifications of the developed coil are as shown in Table 1

Table1. Specifications of the developed coil

r_o	Outer radius of the coil (mm)	11
r_i	Inner radius of the coil (mm)	8
h_{coil}	Height of coil (mm)	30
N_{long}	Number of Longitudinal turns	343
N_{lat}	Number of Lateral turns	23
N_{total}	Total number of turns	7790
R_c	The resistance of the coil (Ω)	1620
L	The inductance of coil (H)	0.45

4.2 Selection of magnet

Alnico, ceramic (hard ferrite), samarium cobalt, and neodymium iron boron NdFeB are the four types of available magnetic materials. Neodymium Iron Boron (NdFeB) magnet is composed of rare earth magnetic material with a high coercive force and strength, and is a relatively low cost, and easy to machine. Hence, a cylindrical magnet of 10 mm diameter and 30 mm height of NdFeB grade 30 material was selected for the electrical coil sub-system.

5. EXPERIMENTAL ANALYSIS

This analysis carried out, to study the effect of various types of shunted electrical loads on the performance of a VBEH

5.1 Frequency response curves (with and without coil magnet system)

Using the experimental setup in Fig. 4, the frequency response curves for the mechanical sub-system are obtained using an ultrasonic sensor for the measurement of the relative displacement between mass m and the base at various values of angular excitation frequency ω in the range of 18 to 21.0 *rad/sec*, shown in Fig. 7.

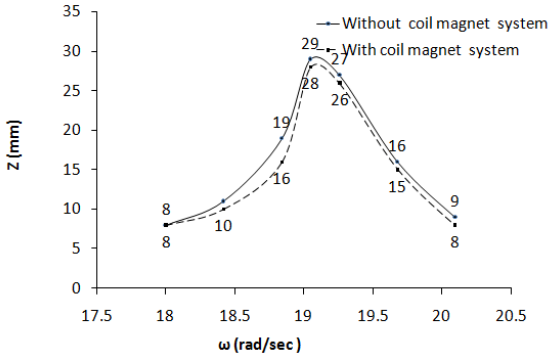

Figure 7. Relative amplitude *Z* vs. Excitation frequency *ω*

Figure 7 shows that the relative amplitude Z is maximum at the resonant frequency for both with and without a coil magnet system as it is expected.

5.2 Open Circuit Voltage *E* Generated Across the Coil

Figure 8 shows the graph of open-circuit voltage E vs. excitation frequency ω.

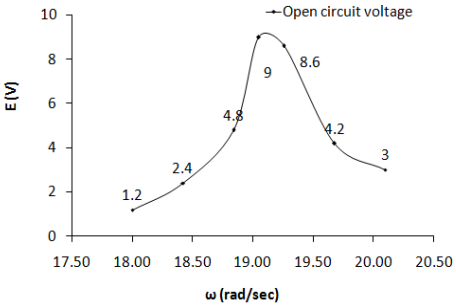

Figure 8. Open circuit voltage *E* vs. Excitation frequency *ω*

The peak voltage, at resonance, recorded across the coil is found to be 9 V.

6. EFFECT OF SHUNTED ELECTRICAL LOADS ON AVERAGE HARVESTED POWER P_{AVEH}

For matched electrical R_L-L-C load circuit of VBEH, the undamped circular natural frequency ω_e of electrical load, a circuit is made equal to the undamped circular natural frequency ω_n of the mechanical sub-system. $\omega_e = \frac{1}{\sqrt{LC}}$, $\omega n = 19.05$ *rad/sec* and $\omega_e = \omega_n$. With value of $L = 0.45H$, the value of C is calculated as $0.006123F$ ($6123\mu F$). The values of L and C varied around these values.

6.1 Voltage V_R across the resistive load R_L

The resistive load R_L connected across the coil is varied as 500 Ω, 1000Ω, 1500Ω, 2000Ω, 3000Ω and 4000Ω. The voltage V_R across R_L measured is by a Digital Storage Oscilloscope (DSO). From Fig.9, it is seen that for an increase in R_L value by 8 times , the increase in V_R is approximately 3 times.

6.2 Average harvested power P_{aveh} at various values of resistive load R_L

From Fig 10 it is seen that the value of P_{aveh} is again maximum at resonance and at R_L = 1600 Ω and P_{aveh} is minimum at 500 Ω.

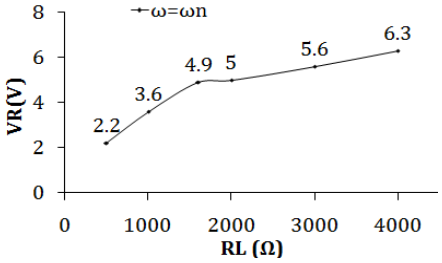

Figure 9. V_R vs. Resistive Load RL, at ω = ω$_n$

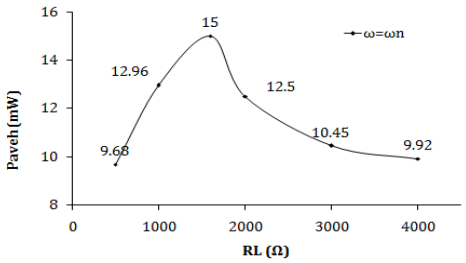

Figure 10. P_{aveh} vs. Resistive Load R_L, at ω = ω$_n$

6.3 Voltage V_R across the various combined values of resistive load and inductive load

Figure 11 shows the combined resistive and inductive electrical load circuit of VBEH. In this case, the load impedance Z_1 due to shunted electrical load (combined resistive and inductive load) given by:

$Z_1 = \sqrt{R_l^2 + x_L^2}$, where R_L is the resistive load and inductance reactance $x_L = \omega_e L$. Figure 12 shows the variable inductance coil.

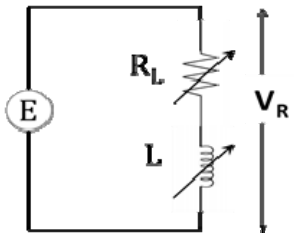

Figure 11. Electrical load circuit

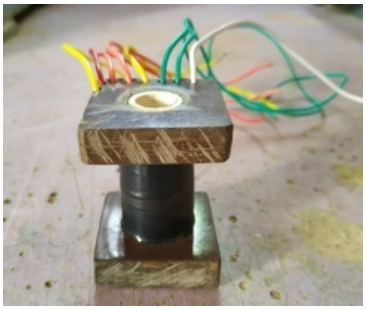

Figure 12. Variable Inductance coil

The values of V_R measured are plotted at different values of Z_1 by varying the excitation frequency.

Table 2. Values of load impedance Z_1 for various values of resistive and inductive loads for $\omega_e = \omega_n$

Sr. No.	Resistive Load $R_L(\Omega)$	Inductance $L(H)$	Reactance $x_L(\Omega)$	Load impedance Z_1 (Ω)
1	400	0.310	5.625	400.3
2	900	0.310	5.625	900.01
3	1600	0.510	9.608	1600
4	2100	0.510	9.608	2100.02
5	2800	0.700	13.188	2800.03

6.4. Average harvested power P_{aveh} at various values of resistive load and inductive load.

Figure 13 shows the curve of peak values of V_R vs. Z_1, and Fig 14 shows the curve of values of P_{aveh} vs. Z_1 at resonance, respectively.

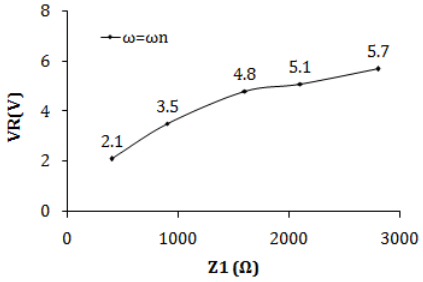

Figure 13. V_R vs. Load Impedance Z_1, at t

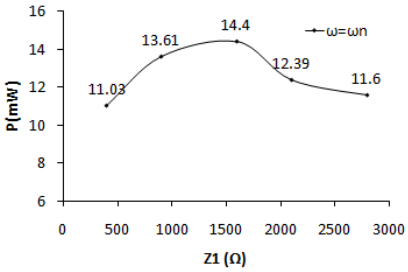

Figure 14. P_{aveh} vs. Load Impedance Z_1, at ω = ω$_n$

Figure 13 shows that with the increase in the Z_1, the voltage V_R increases. Figure 14 shows that the P_{aveh} is maximum at Z_1 = 1600 Ω, and its value is 14.40 mW.

6.5. Voltage V_R across the various combined values of resistive load R_L, inductive load, and capacitive load.

Figure 15 shows the combined resistive, inductive, and capacitive electrical load circuit of the VBEH. In this case, the load impedance Z_2 due to shunted electrical load (combined resistive, inductive, and capacitive load) given by:

$$Z_2 = \sqrt{R_L^2 + (x_L - x_c)^2}$$

where, R_L is the resistive load, inductance reactance x_L = $\omega_e L$, and capacitive reactance $x_c = \frac{1}{\omega_e c}$, where c is capacitance. The values of load impedance Z_2 for various values of resistive, inductive, and capacitive loads are tabulated in Table 3. Figures 16 (a) and 16 (b), show the variable inductance coil and capacitors, respectively.

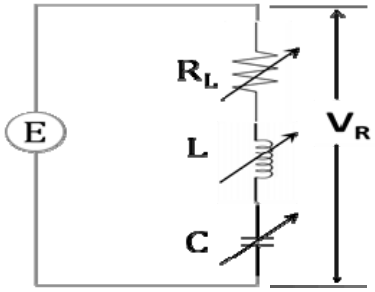

Figure 15. Electrical load circuit

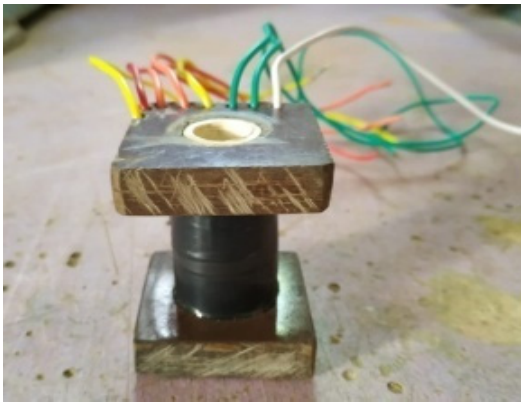

Figure 16. (a) Variable Inductance coil

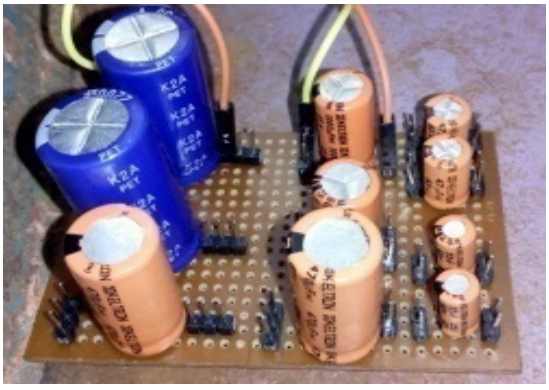

Figure 16. (b) capacitors

Table 3. Values of load impedance Z_2 for various values of resistive, inductive and capacitive loads for $\omega_e = \omega_n$

Sr.	Resistive Load $R_L(\Omega)$	Inductance $L(H)$	Capacitance $c(F)$	Load impedance $Z_2(\Omega)$
1	400	0.310	0.0032	400.14
2	900	0.310	0.0044	900.01
3	1600	0.510	0.0054	1600
4	2100	0.510	0.0064	2100.12
5	2800	0.700	0.0069	2800.03

Table 3 gives the values of load impedance Z_2. The curves of V_R vs. excitation frequency ω for the various value of Z_2 plotted.

6.6 Average power harvested P_{aveh} at different values of Z_2

The effect of varying the value of Z_2 (at resonance) on V_R and P_{aveh} are respectively shown in Fig. 17 and Fig. 18. Figure 17 reveals that V_R is maximum (5.5V) at $Z_2 = 2800\Omega$ and Fig.18 reveals that P_{aveh} is maximum ($13.81mW$) at $Z_2 = 1600\Omega$.

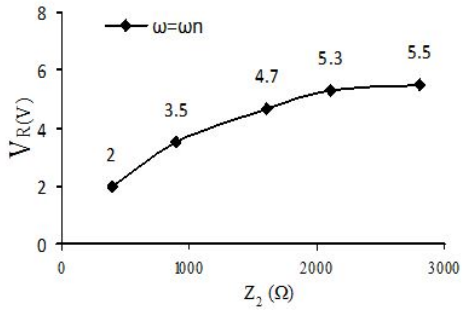

Figure 17. V_R vs. Load Impedance Z_2, at $\omega = \omega_n$

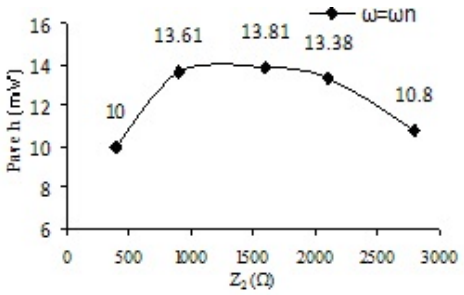

Figure 18. P_{aveh} vs.Load Impedance Z_2, at $\omega = \omega_n$

7. DISCUSSION OF RESULTS

The comparison of the results shown in figures 9,13,and 17 for the voltage V_R across the resistance of the value R_L, Z_1, and Z_2 shows that as the resistive load R_L increases the voltage V_R , at resonance, increases quickly up to R_L =1600Ω, $Z_1 \approx 1600\ \Omega$ and $Z_2 \approx 1600\ \Omega$. For the various values R_L, Z_1, and Z_2 greater than 1600Ω, the voltage increases steadily.

From the comparison of the results shown in the figures 10, 14, and 18, it can be seen that average power harvested P_{aveh} is maximum at or near the value of $Z_1 \approx 1600\ \Omega$ and $Z_2 \approx 1600\ \Omega$.The effect of the addition of inductive and capacitive load is to widen the range of values of load impedances at which the maximum P_{aveh} is obtained. Also, it is seen that the values of V_R and P_{aveh} are maximum at or near R_L =1600 Ω or $Z_1 \approx 1600\ \Omega$ or $Z_2 \approx 1600\ \Omega$ which is very close to the internal resistance of the coil of the electromagnetic sub-system.

7.1 Average generated power p_{ave} from VBEH

Equation (2) of section 3 gives the average generated power P_{ave} from VBEH. In Eq. (2), m is the harvester mass, ω is the excitation frequency, ω_n is the undamped circular natural frequency of the mechanical sub-system, Y is the amplitude of excitation, ζ_m is the mechanical damping ratio, and ζ_m the electrical damping ratio.

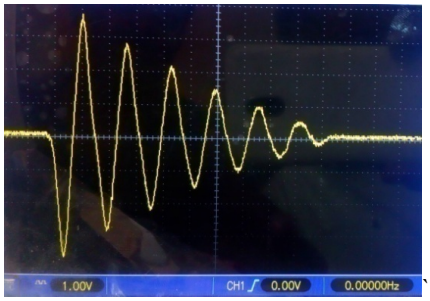

Figure 19. Open circuit voltage E vs. time t

Eq.(2) shows that P_{ave} is controlled by ζ_e, therefore, the experimental determination of ζ_e is carried out by the procedure outlined in the next section.

7.2 Experimental determination of ζ_m

Using the experimental setup developed for VBEH (without electrical load), a transient response curve E (open-circuit voltage) vs. time t, as shown in Fig. 19 is obtained using a digital storage oscilloscope (screen-shot). From this curve, ζ_m was determined using the method of logarithmic decrement and is found to be 0.025.

7.2 Experimental determination of ζ_m (Method 1)

Using the experimental setup developed for VBEH (with an electrical resistive load of 1600 Ω), a transient response curve V_R (voltage across resistive load) vs. time t, as shown in Fig. 20, is obtained using a digital storage oscilloscope (screenshot). From this curve, using the method of logarithmic decrement, the total damping ratio ζ was determined and it is found to be 0.03. Now, $\zeta = \zeta_m + \zeta_e$. With $\zeta = 0.03$ and $\zeta_m = 0.025$ from method 1, the electrical damping ratio ζ_e obtained as 0.005, and is denoted as ζ_{e1}.

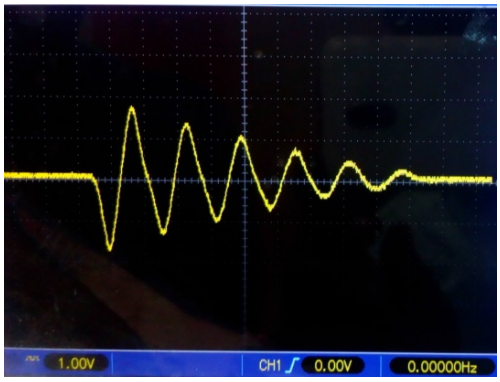

Figure 20. Voltage V_R vs. time t

7.3 Determination of Electrical damping ratio ζ_e (Method 2)

The electrical damping ratio calculated as [11]

$$\zeta_e = \frac{\left(N_{total} B L_1\right)^2}{2m\omega_n \left(R_c + R_L\right)} \tag{4}$$

In Eq. (4), N_{total} is the total number of turns, $L_1$is length of the coil, m is mass, ω_n is circular natural frequency, R_C is the resistance of the coil, R_L is the resistive load, and B is the magnetic flux density in the direction of the axis of the magnet. The value is calculated, as explained by Halim et al. [10]. The magnetic flux density B is given by Eq. (5).

$$B = \frac{B_r}{2}\left[\frac{h_{mag}+x}{\sqrt{R_{mag}^2+\left(h_{mag}+x\right)^2}} - \frac{x}{\sqrt{R_{mag}^2+x^2}}\right] \tag{5}$$

At $x=0$, i.e. at the point near the magnet pole face, the value of B is maximum. For the developed VBEH, a cylindrical NdFeB magnet of height h_{mag}=0.03m, radius R_{mag}= 0.005m, and having the residual magnetic flux density $B_r = 0.8T$ was selected. Substituting these values of h_{mag}, R, and Br. in Eq. (5), the value of B at pole face ($x=0$) is found to be 0.39T.

The value of B is also determined using the standard Tesla meter setup, as shown in Fig.21. Figure 22 shows the curves of experimental magnetic flux density B vs. distance x from the magnet pole face for the magnets measuring 4 mm and 5 mm in radius.

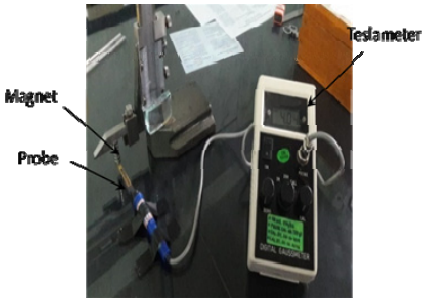

Figure 21. Teslameter setup

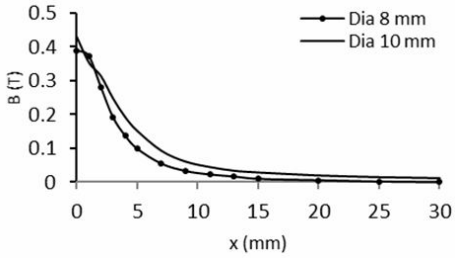

Figure 22. Flux density *B* vs. Distance *x* from pole face

The experimental value of B for 10mm diameter NdFeB magnet is obtained as 0.44T. The value of B obtained from Eq. (05) is in close agreement with that obtained from experimental measurement. Using the values $B = 0.44$T, $N = 7790$, $L_1 = 0.019$ m, $m = 4.31$ kg, $\omega_n = 10.05$ rad/sec, $Rc = 1620$ Ω, and R_L=1600 Ω in Eq. (4), The value of ζ_e from method 2 is obtained as 0.008, and is denoted as ζ_{e2}.

The analytical expression for the electrical damping factor c_e is obtained by equating the power dissipation in the coil and shunted electrical load impedance to that obtained from the electromagnetic force. The electrical damping ratio ζe is obtained as $\zeta_e = \frac{c_e}{2m\omega_n}$.

From the expression for the ζ_e, in Equ. 4, it can be seen that for the given coil magnet configuration, size, and for the value of natural frequency of the mechanical sub-system (tuned to excitation frequency of the ambient vibration) the value of ζ_e is dominated by the value of load resistance. Thus as the shunted electrical load increases the value of ζ_e decreases, and the value of total damping ratio ζ decreases, resulting in more harvested power from VBEH.

7.4 Average Generated Power P_{ave} from the developed VBEH.

The plot of P_{ave} vs. ω is, obtained and is as shown in Fig. 23**.** Substituting the values $m = 4.31$kg, $\omega_n = 19.05$ rad/s, $\zeta_m = 0.025$, $Y = 0.001$m and $\zeta_e = \zeta_{e1} = 0.005$ in Eq. (2), and varying the excitation frequency ω in the range of 17.50 to 20.50 rad/sec.

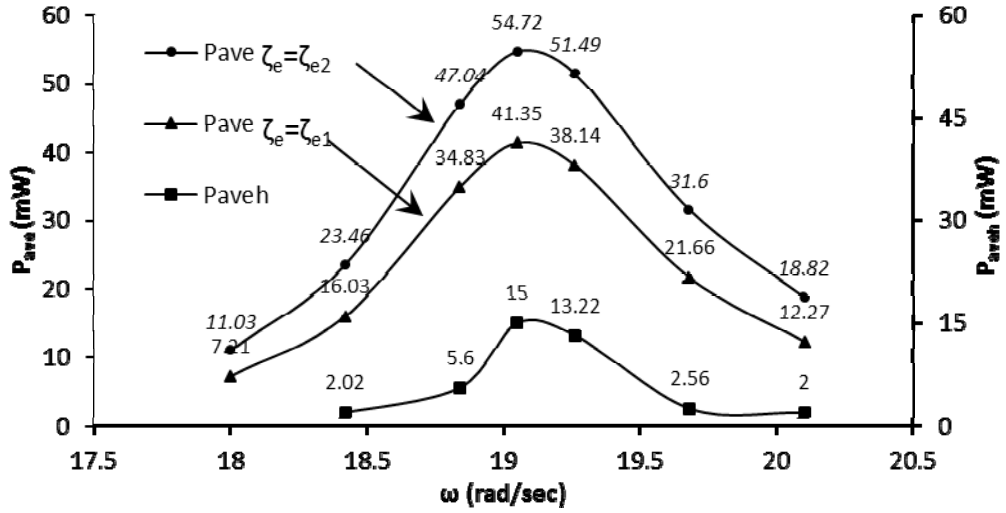

Figure 23. Average generated power P_{ave} (when $\zeta_e=\zeta_{e1}$) vs. excitation frequency ω, Average generated power P_{ave} (when $\zeta_e=\zeta_{e2}$) vs. excitation frequency ω, Average harvested power P_{aveh} vs. excitation Frequency ω, (at the resistive load of 1600Ω).

Figure 23 shows the curve of P_{ave} vs., excitation frequency ω, for $\zeta_e=\zeta_{e1}$= 0.005 and of P_{ave} vs. excitation frequency ω, for $\zeta_e=\zeta_{e2}$= 0.008, for the resistive load of 1600Ω which is approximately equal to the internal resistance of the coil. The figure shows that the value of the average generated power P_{ave} based on the electrical damping ratio ζ_{e1} (method 1) is less than that obtained using the analytical formula for ζ_{e2} (method 2). Figure 23 also shows the curve of average harvested power P_{aveh} vs. excitation frequency ω. From the figure, it is seen that average harvested power P_{aveh} is maximum, at the resonant frequency, for the resistive load of 1600Ω. The average harvested power P_{aveh} is much less than the average generated power P_{ave}.

8. CONCLUSIONS

From the results obtained from the experiments and mathematical equations, the following conclusions are drawn.

1. The effect of variation of shunted electrical loads R_L (resistive), Z_1 (resistive and inductive) and Z_2 (resistive, inductive and capacitive) on the average harvested power P_{aveh} is investigated at various excitation frequencies. It shows that the average harvested power P_{aveh} is maximum at resonance. The P_{aveh} decreases with an increase in electrical load on the harvester. It shows that the value of P_{aveh} is maximum at the resistive load of 1600Ω. This research work is in line with the research results reported in the state-of-the-art of the design and development of vibration-based energy harvesters.
2. Using the transient response curve of open-circuit voltage E vs. time t, the mechanical damping ratio ζ_m is estimated as 0.025, and Using the transient response curve of V_R vs. time t, total damping ratio ζ is determined as 0.03, at the resistive load of 1600Ω. From the estimated values of ζ and ζ_m, the electrical damping ratio ζ_{e1} was calculated as $\zeta_{e1} = \zeta - \zeta_m = 0.005$, (method 1 of section 7.2) . Also the value $\zeta_e = \zeta_{e2} = 0.008$ was estimated using the analytical formula for ζ_e [11]. It shows that the value of electrical damping ratio $\zeta_e = \zeta_{e1}$, obtained from method 1 of section 7.2, is less than that obtained from the analytical formula for ζe using method 2 of section 7.3.The experimental value of electrical damping ratio ζ_e (0.005) is very small as compared to the value of mechanical damping ratio ζ_m (0.025). This is desirable to obtain maximum harvester power from a VBEH. This result will undoubtedly be beneficial in the design and development of vibration-based energy harvesters.
3. The value of the average generated power P_{ave} based on the electrical damping ratio ζ_{e1} (method 1) is less than that obtained using the analytical formula for ζ_e (method 2). The values of the average generated power P_{ave} and average harvested power P_{aveh} of VBEH are maximum when the value of excitation frequency equals the natural frequency of the mechanical sub-system of the VBEH. These results bring out the importance of the experimental determination of the electrical damping ratio in the maximization of the output power of the VBEH shunted to electrical loads.

DECLARATION OF CONFLICT OF INTEREST

The author(s) declared no potential conflict of interest in regard to the research, authorship and/or publication of this article

FUNDING INFORMATION

The author(s) received no financial support for the study, authorship, and publication of this article.

REFERENCES

[1] C. B. Williams and R. B. Yates, “Analysis of a micro-electric generator for microsystems,” Sensors Actuators, A Phys., vol. 52, no. 1–3, pp. 8–11, 1996.

[2] C. B. Williams, C. Shearwood, M. A. Harradine, P. H. Mellor, T. S. Birch, and R. B. Yates, “Development of electromagnetic micro-generator.”IEE proc.circuits devices Syst,vol.148, No.6,pp,337-342,2001.

[3] S. Roundy, P. K. Wright, and J. Rabaey, “A study of low-level vibrations as a power source for

wireless sensor nodes," Comput. Commun., vol. 26, no. 11, pp. 1131–1144, 2003.
[4] N. G. Stephen, "On the maximum power transfer theorem within electromechanical systems," Proc. Inst. Mech. Eng. Part C J. Mech. Eng. Sci., vol. 220, no. 8, pp. 1261–1267, 2006.
[5] N. G. Stephen, "On energy harvesting from ambient vibration," J. Sound Vib., vol. 293, no. 1–2, pp. 409–425, 2006.
[6] D. Spreemann, D. Hoffmann, B. Folkmer, and Y. Manoli, "Numerical optimization approach for resonant electromagnetic vibration transducer designed for random vibration," J. Micromechanics Microengineering, vol. 18, no. 10, 2008.
[7] B. L. Ooi, J. M. Gilbert, and A. R. A. Aziz, "Switching damping for a frequency-tunable electromagnetic energy harvester," Sensors Actuators, A Phys., vol. 234, pp. 311–320, 2015.
[8] Z. Szabo, P. Fiala, and P. Dohnal, "Magnetic circuit modifications in resonant vibration harvesters," Mech. Syst. Signal Process., vol. 99, pp. 832–845, 2018.
[9] S. Naifar, S. Bradai, C. Viehweger, and O. Kanoun, "Survey of electromagnetic and magnetoelectric vibration energy harvesters for low-frequency excitation," Meas. J. Int. Meas. Confed., vol. 106, pp. 251–263, 2017.
[10] M. A. Halim and J. Y. Park, "Modeling and experiment of a handy motion driven, frequency up-converting electromagnetic energy harvester using transverse impact by the spherical ball," Sensors Actuators, A Phys., vol. 229, pp. 50–58, 2015.
[11] M. A. Halim, H. Cho, and J. Y. Park, "Design and experiment of a human-limb driven, frequency up-converted electromagnetic energy harvester," Energy Convers. Manag., vol. 106, pp. 393–404, 2015.
[12] H. Zhang, L. R. Corr, and T. Ma, "Effects of electrical loads containing non-resistive components on piezoelectric energy harvesting," Mech. Syst. Signal Process., vol. 111, pp. 210–221, 2018.
[13] W. C. Tai and L. Zuo, "On the optimization of energy harvesting from base-excited vibration," J. Sound Vib., vol. 411, pp. 47–59, 2017.
[14] G. Caruso, "Broadband energy harvesting from vibrations using magnetic transduction," J. Vib. Acoust. Trans. ASME, vol. 137, no. 6, pp. 1–4, 2015.
[15] K. Ashraf, M. H. Md Khir, J. O. Dennis, and Z. Baharudin, "Improved energy harvesting from low-frequency vibrations by resonance amplification at multiple frequencies," Sensors Actuators, A Phys., vol. 195, pp. 123–132, 2013.
[16] L. Simeone, M. Ghandchi Tehrani, and S. Elliott, "Level-dependent load in a pendulum-like energy harvester," Mech. Syst. Signal Process., vol. 119, pp. 244–254, 2019.
[17] L. Zuo and W. Cui, "Dual-functional energy-harvesting and vibration control: Electromagnetic resonant shunt series tuned mass dampers," J. Vib. Acoust. Trans. ASME, vol. 135, no. 5, pp. 1–9, 2013.
[18] Y. Liu, C. C. Lin, J. Parker, and L. Zuo, "Exact H2 Optimal Tuning and Experimental Verification of Energy-Harvesting Series Electromagnetic Tuned-Mass Dampers," J. Vib. Acoust. Trans. ASME, vol. 138, no. 6, 2016.
[19] X. Tang and L. Zuo, "Enhanced vibration energy harvesting using dual-mass systems," J. Sound Vib., vol. 330, no. 21, pp. 5199–5209, 2011.
[20] S. F. ul H. Gilani, M. H. bin M. Khir, R. Ibrahim, E. ul H. Kirmani, and S. I. ul H. Gilani, "Modelling and development of a vibration-based electromagnetic energy harvester for industrial centrifugal pump application," Microelectronics J., vol. 66, no. April, pp. 103–111, 2017.
[21] Y. Tadesse, Shujun Zhang, and S. Priya, "Multimodal energy harvesting system: Piezoelectric and electromagnetic," J. Intell. Mater. Syst. Struct., vol. 20, no. 5, pp. 625–632, 2009.
[22] V. Bhatnagar and P. Owende, "Energy harvesting for assistive and mobile applications," Energy Sci. Eng., vol. 3, no. 3, pp. 153–173, 2015.
[23] H. Wang, A. Jasim, and X. Chen, "Energy harvesting technologies in roadway and bridge for different applications – A comprehensive review," Appl. Energy, vol. 212, no. December 2017, pp. 1083–1094, 2018.
[24] X. Zhang, Z. Zhang, H. Pan, W. Salman, Y. Yuan, and Y. Liu, "A portable high-efficiency electromagnetic energy harvesting system using supercapacitors for renewable energy applications in railroads," Energy Convers. Manag., vol. 118, pp. 287–294, 2016.
[25] G. Gatti, M. J. Brennan, M. G. Tehrani, and D. J. Thompson, "Harvesting energy from the vibration of a passing train using a single-degree-of-freedom oscillator," Mech. Syst. Signal Process., vol. 66–67, pp. 785–792, 2016.
[26] L. Zuo and P. S. Zhang, "Energy harvesting, ride comfort, and road handling of regenerative vehicle suspensions," J. Vib. Acoust. Trans. ASME, vol. 135, no. 1, pp. 1–8, 2013.
[27] S. Chamanian, S. Baghaee, H. Ulusan, Ö. Zorlu, H. Külah, and E. Uysal-Biyikoglu, "Powering-up wireless sensor nodes utilizing rechargeable batteries and an electromagnetic vibration energy harvesting system," Energies, vol. 7, no. 10, pp. 6323–6339, 2014.
[28] T. Yildirim, M. H. Ghayesh, W. Li, and G. Alici, "A review on performance enhancement techniques for ambient vibration energy harvesters," Renew. Sustain. Energy Rev., vol. 71, no. December 2016, pp. 435–449, 2017.
[29] A. R. El-Sayed, K. Tai, M. Biglarbegian, and S. Mahmud, "A survey on recent energy harvesting mechanisms," Can. Conf. Electr. Comput. Eng., vol. 2016-October, pp. 0–4, 2016.
[30] P. V. Malaji and S. F. Ali, "Broadband energy harvesting with mechanically coupled harvesters," Sensors Actuators, A Phys., vol. 255, pp. 1–9, 2017.
[31] Pengwei Li, Ying Liu, Yanfen Wang, Cuixian Luo, Gang Li, Jie Hu, Wei Liu and Wendong Zhang "Low-frequency and wideband vibration energy harvester with flexible frame and interdigital

structure," AIP Adv., vol. 5, no. 4, 2015.
[32] J. Siang, M. H. Lim, M. Salman Leong, "Review of vibration-based energy harvesting technology: Mechanism and architectural approach," Int. J. Energy Res., vol. 42, no. 5, pp. 1866–1893, 2018.
[33] H. A. Wheeler, "Simple inductance formulas for radio coils," Proc. Inst. Radio Eng., vol. 16, no. 10, pp. 1398–1400, 1928.

NOMENCLATURE

N	Speed rpm
z	Relative displacement of mass w.r.t.base
$\dot{z}$	Relative velocity of mass w.r.t.base
$\ddot{z}$	Relative acceleration of mass w.r.t.base
ω	Circular excitation frequency, rad/sec
ω_n	Circular natural frequency rad/sec
$\frac{\omega}{\omega_n}$	Frequency ratio
m	Mass, Kg
K	Spring rate, N/m
c_m	Mechanical damping coefficient
c_e	Electrical damping coefficient
c	Damping coefficient $c= c_m + c_e$
ζ_m	Mechanical Damping ratio.
ζ_e	Electrical damping ratio.
ζ	Damping ratio = $\zeta_m + \zeta_e$
X	Displacement amplitude of mass, m
Y	Amplitude base excitation, m
Z	Relative amplitude(X-Y), m
Z_1	load Impedance, Ω
Z_2	Impedance load , Ω
E	Open circuit Voltage, V
V_R	Voltage across the load resistance, V
P_{ave}	Average generated Power, mW
P_{aveh}	Average harvested Power, mW
ω_e	Circular natural frequency of the electrical circuit, rad/sec
B	Magnetic flux density, T
B_r	Residual magnetic flux density ,T
h_{mag}	Height of magnet, m
R_{mag}	Radius of the magnet m
x	Distance from magnet pole face, m
R_L	Resistive load Ω
L	Inductive load H
C	Capacitive load F

ЕКСПЕРИМЕНТАЛНО ИСТРАЖИВАЊЕ УТИЦАЈА ПАРАЛЕЛНИХ ЕЛЕКТРИЧНИХ ОПТЕРЕЋЕЊА НА ПЕРФОРМАНСЕ ЕЛЕКТРОМАГНЕТНОГ САКУПЉАЧА ЕНЕРГИЈЕ БАЗИРАНОГ НА ВИБРАЦИЈАМА

В.Б. Патил, М. Сакри

Данас се истраживачи хватају у коштац са проблемима максимизирања излазне снаге код електромагнетног сакупљача енергије базираног на вибрацијама (ВБЕХ). Параметри који утичу на излазну снагу ВБЕХ-а су: однос електричног пригушења (ζ_e), однос механичког пригушења ($\zeta_м$) и импеданса оптерећења паралелног електричног оптерећења. Зато је обављено експериментално истраживање утицаја паралелног електричног оптерећења на излазну снагу ВБЕХ-а и одређивање ζ_e који максимизира излазну снагу. ВБЕХ је дизајниран и развијен да би се добио висок напон отвореног кола. Утицај отпорног, индуктивног и капацитативног оптерећења на излазну снагу ВБЕХ-а је истражен помоћу експеримента постављеног за наведене параметре. Утврђено је да је излазна снага ВБЕХ-а максимална при резонантној фреквенцији, када је еквивалентна импеданса оптерећења једнака унутрашњем отпору електромагнетног калема и када је вредност ζ_e веома мала у односу на вредност $\zeta_{м.}$